15-7-1996

Spectroscopy and piezospectroscopy of the Lyman transitions and Fano resonances of indium in silicon

G. Piao
University of Wollongong

R. A. Lewis
University of Wollongong, roger@uow.edu.au

P. Fisher
University of Wollongong, pfisher@uow.edu.au

Spectroscopy and piezospectroscopy of the Lyman transitions and Fano resonances of indium in silicon

G. Piao, R. A. Lewis, and P. Fisher
Department of Physics, University of Wollongong, Wollongong, New South Wales 2522, Australia
(Received 30 October 1995; revised manuscript received 20 February 1996)

A spectroscopic investigation has been made of the $p_{3/2}$ and $p_{1/2}$ transitions and the bound hole associated Fano resonances of indium in silicon. Accurate values have been obtained for the transition energies of many lines. The parameters characterizing the Fano resonances have been determined and the behavior of the Fano resonances under uniaxial stress has been studied. The Fano resonances show a stress splitting similar to that of their $p_{3/2}$ counterparts. Detailed piezospectroscopic data for the lines 1, 2, 3, 4, $4A$, $2p'$, and $3p'$ under $\langle 111\rangle$, $\langle 110\rangle$, and $\langle 100\rangle$ compression permit a more accurate determination of deformation potential constants than previously obtained (with some significant differences) and the determination of some previously unknown deformation potential constants. [S0163-1829(96)04027-1]

I. INTRODUCTION

Substitutional group III acceptors in silicon, such as indium, bind one hole and produce a solid-state analog of the hydrogen atom. For indium impurity, three main series of excitations can be observed in the mid-infrared spectral region 140–220 meV. The $p_{3/2}$ series originates in transitions from the hole ground state to bound states associated with the $j=3/2$ valence band. The $p_{1/2}$ series comprises transitions from the hole ground state to bound states associated with the $j=1/2$ valence band; these transitions are in resonance with the $p_{3/2}$ photoionization continuum. The ionization limits of these two Lyman series differ by the spin-orbit split-off band spacing of ~ 44 meV. The Fano series arises from compound states involving a bound hole to bound hole $p_{3/2}$ transition and a phonon. This series is separated in energy from the $p_{3/2}$ series by the energy of the silicon zone-center optical phonon $\hbar\omega_{\rm opt}$ of ~ 64 meV.

Early experimental investigations of the $p_{3/2}$ excitation spectra of group III impurities in silicon[1,2] demonstrated the correspondence of excited-state energy levels and the chemical shift in the ground states between different species — the larger the acceptor atom, the higher the ionization energy. Both the $p_{1/2}$ series, first observed for boron in silicon,[3] and the $p_{3/2}$ series have now been studied at high resolution yielding very rich spectra.[4–6] Piezospectroscopic investigations of the $p_{3/2}$ and $p_{1/2}$ spectra of indium (and other acceptors) in silicon have been carried out by Onton, Fisher, and Ramdas[2] and Chandrasekhar *et al.*[7] Their systematic work has contributed largely to the present understanding of the energies, symmetries, and stress behaviors of the ground and lower excited states of indium in silicon.

The interference of a discrete energy level with a continuum of levels results in an asymmetric spectroscopic feature known as a Fano resonance.[8] Fano resonances have been observed for both donors and acceptors in both silicon and germanium. In the absorption spectrum of indium in silicon, Fano resonances were first reported by Bhatia,[9] but the spectrum shown in that work has not been reproduced in later similar measurements[10] and differs from the features observed in this investigation. Fano resonances have also been observed in the photoconductivity spectrum of indium in silicon.[10,11] The shapes of the features in photoconductivity are rather different from those seen in absorption due to differences in the mechanisms governing the resonant process and its detection.[12]

Calculations of the energies of shallow acceptors in semiconductors have been carried out within the framework of the effective-mass approximation. Baldereschi and Lipari separated the Hamiltonian into a spherical term[13] and a cubic term[14] to assist in the calculation and the interpretation of the results. Further work by Baldereschi and co-workers has refined and extended this approach.[15–18] Similar variational calculations have been undertaken by Buczko[19] and Buczko and Bassani.[20] Polupanov and others have developed a nonvariational method of solving the Hamiltonian.[21–27] The most detailed results from each of these approaches have yielded oscillator strengths, as well as energies, for group III shallow impurities in Si;[28–30] no calculations specifically for indium impurity have been reported to our knowledge. Group theoretical techniques have been used to determine the effect of deformations on cubic crystals in general,[31] and on impurities therein.[2,32–34] The relative intensities of transitions between states of the relevant symmetries have been determined. Numerical calculations of the deformation potential constants of some acceptor states in silicon and germanium have been carried out by Buczko.[19]

In this investigation, the use of some samples with low concentrations of indium and higher-resolution measurements than those employed in previous studies[2,7] have permitted more detailed piezospectra to be obtained. This has allowed clarification of some of the ambiguities and a more accurate determination of the deformation potential constants. Using an analytical method described previously,[35] the parameters[8] q, Γ, and f have been determined for some of the Fano resonances. Piezospectroscopic observations on the Fano resonances have been made in this impurity system. Good correlation with the $p_{3/2}$ series is exhibited.

II. EXPERIMENTAL PROCEDURES

The indium-doped silicon samples used in this investigation had room-temperature carrier concentrations in the

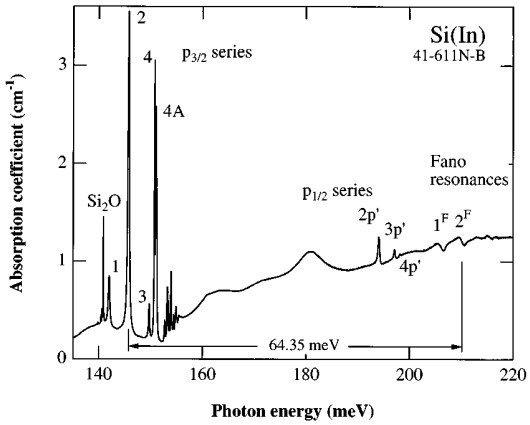

FIG. 1. Unperturbed spectrum of Si(In), showing $p_{3/2}$, $p_{1/2}$, and Fano series. The coolant used was liquid helium. Room-temperature carrier concentration was $\sim 6\times10^{15}$ cm^{-3}.

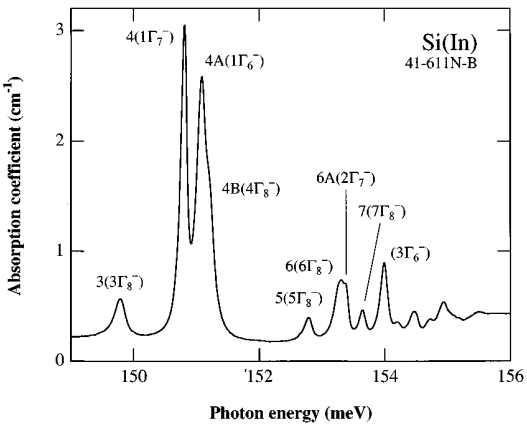

FIG. 2. Details of the high-energy portion of the unperturbed $p_{3/2}$ series of Fig. 1.

range $\sim 5\times10^{15}$ to $\sim 2\times10^{16}$ cm^{-3}. Two samples were prepared from a float zone silicon crystal (ingot 41-611N) and another two from a crucible grown boule (ingot 2789) (see Sec. VI). Liquid helium was used as the coolant. Absorption spectra were obtained using a Bomem DA3.26 Fourier transform infrared spectrometer. All spectra were measured using a mirror travel of 2.5 cm, giving an unapodized resolution of 0.15 cm^{-1} ($\sim$19 μeV). The widths of the absorption lines are such that the use of the highest resolution of the spectrometer ($\sim$2 μeV) was not justified. It might be noted that the $p_{3/2}$ lines of group III acceptors in silicon are significantly broader than are those for these impurities in germanium; the reason for this is not known. Uniaxial compression was applied to the samples by employing calibrated lead weights. Details of the low-temperature quantitative stress cryostat and the mounting technique have been described elsewhere.[36–38]

III. ZERO STRESS SPECTRA

The optical absorption spectrum of indium in silicon in the region 140–220 meV is shown in Fig. 1. In the spectrum can be seen, in order of increasing energy, an oxygen vibrational band ($\sim$141 meV), the $p_{3/2}$ series ($\sim$142–156 meV), the $p_{1/2}$ series ($\sim$194–198 meV), and the Fano resonances ($\sim$203–220 meV). Figure 2 displays an enlarged portion of the $p_{3/2}$ spectrum. In Figs. 1 and 2 the $p_{3/2}$ excitation lines are labeled in order of increasing energy following the notation of Onton, Fisher, and Ramdas[2] while the $p_{1/2}$ spectral lines are labeled using the notation of Zwerdling *et al.*[3] The Fano series is separated in energy from the associated $p_{3/2}$ series by 64.35 meV, the energy of the zone-center optical phonon in silicon,[39] as indicated in Fig. 1.

The $p_{3/2}$ and $p_{1/2}$ spectra are essentially similar to those reported previously;[4,6] the spectrum of Pajot *et al.*[6] is slightly superior to the present one. The measured energies for the various states are given in Table I.

Also given in Table I are the assigned symmetry labels, which will be discussed later in greater detail with reference to the stress behavior of the transitions; some of these labels are given in Fig. 2. The first three lines, which are given the experimental labels 1, 2, and 3, are unambiguously identified with transitions from the ground state to the final states $1\Gamma_8^-$, $2\Gamma_8^-$, and $3\Gamma_8^-$,[40] respectively.

The triplet structure of line 4 is evident in Fig. 2. Lines 4*A* and 4*B* are unresolved due to their intrinsic width. This asymmetric doublet has been resolved by curve fitting by Covington, Harris, and Spry[41] and Tardella and Pajot.[4] Both studies found the separation of the doublet to be 0.9 cm^{-1}, while curve fitting to the present spectrum yields 0.99 $\pm$0.10 cm^{-1} (0.12$\pm$0.01 meV). Similarly, the energy separation of the closely spaced lines 6 and 6*A* was determined here by curve fitting to be 0.67$\pm$0.20 cm^{-1} (0.08$\pm$0.02 meV). The main uncertainty in the present values comes from the slightly asymmetric line shapes.

The closely spaced structure of line 4 is similar to, although not precisely of the same origin as, the structure of line C of acceptors in germanium.[42,43] In silicon, the presence of the triplet is rather atypical because of the strong band warping.[28] The final states of the transitions contributing to this triplet structure in silicon are predicted by theory to be $1\Gamma_6^-$, $1\Gamma_7^-$, and $4\Gamma_8^-$.[20,28,30] The $4\Gamma_8^-$ state is commonly calculated as having the smallest binding energy of the three and is assigned to the final state of the 4*B* transition. However, there is a difference in the predicted order of the energies of the $1\Gamma_6^-$ and $1\Gamma_7^-$ states depending upon the calculation. Binggeli and Baldereschi[28] calculated the binding energy of the $1\Gamma_6^-$ state to be almost equal to but slightly larger than that of the $1\Gamma_7^-$ state; the opposite ordering is given by Buczko and Bassani,[20] and by Beinikhes *et al.*[30]

The difference, as calculated by various workers, in the predicted intensities of the optical transitions from the ground state to these final states is large. The ratios of the line intensities of the three components 4, 4*A*, and 4*B* have been given as 100:92:33 (Ref. 28) and as 11:22:8.[30] From curve fitting to the spectrum of Fig. 2, the ratios 100:89:49 have been obtained, which are closer to those of Binggeli and Baldereschi.[28] No firm experimental conclusion can be drawn from the unperturbed spectrum for the symmetry assignment of these states. This ambiguity will be resolved later in considering the behavior of the transitions under an applied stress.

Line 5 is unambiguously associated with the $5\Gamma_8^-$ final state. Theory predicts two closely spaced states next, viz.,

TABLE I. Experimental and theoretical energies (in meV) of indium in silicon. The data are correlated with the final states (column 4), which are given in the order of their energy as calculated in Ref. 29.

Transitions			Final states				
	Energies				Energies		
Label	This work[a]	Ref. 6	Label	Theory Ref. 29	This work[b]	Theory Ref. 30	This work[c]
1	142.023	142.04	$1\Gamma_8^-$	−15.63	−15.60	−15.79	−14.95
2	145.791	145.81	$2\Gamma_8^-$	−11.54	−11.59	−11.48	−11.18
3	149.787	149.81	$3\Gamma_8^-$	−7.35	−7.34	−7.24	−7.19
4	150.809	150.83	$1\Gamma_7^-$	−6.08	−6.25	−6.23	−6.17
4*A*	151.083	151.11	$1\Gamma_6^-$	−5.98	−5.96	−6.18	−5.89
4*B*	151.21	151.18	$4\Gamma_8^-$	−5.86	−5.83	−5.95	−5.76
5	152.785	152.81	$5\Gamma_8^-$	−4.17	−4.15	−4.24	−4.19
		153.32	$2\Gamma_6^-$	−3.70		−3.81	
6	153.29		$6\Gamma_8^-$	−3.63	−3.62	−3.84	−3.69
6*A*	153.38	153.40	$2\Gamma_7^-$	−3.50	−3.52	−3.62	−3.60
7	153.645	153.67	$7\Gamma_8^-$	−3.24	−3.24	−3.33	−3.33
8	153.99	154.01	$3\Gamma_6^-$	−2.88	−2.87	−2.97	−2.98
			$3\Gamma_7^-$	−2.86		−3.07	
	154.208		$8\Gamma_8^-$	−2.66	−2.64	−2.85	−2.77
		154.23	$9\Gamma_8^-$	−2.43		−2.70	
		154.23	$4\Gamma_6^-$	−2.43		−2.77	
	154.47	154.01	$4\Gamma_7^-$	−2.35	−2.36	−2.88	−2.51
		154.46	$10\Gamma_8^-$	−2.29		−2.61	
	154.72		$11\Gamma_8^-$	−2.12	−2.10	−2.44	−2.26
			$5\Gamma_6^-$	−1.96		−2.41	
			$12\Gamma_8^-$	−1.91		−2.36	
	154.94	154.51	$5\Gamma_7^-$	−1.87	−1.86	−2.50	−2.04
		154.74	$13\Gamma_8^-$	−1.85		−2.17	
		154.89	$6\Gamma_6^-$	−1.76		−2.07	
		154.96	$6\Gamma_7^-$			−2.04	
		155.04	$14\Gamma_8^-$			−1.95	
		155.13	$7\Gamma_6^-$			−1.93	
		155.13	$7\Gamma_7^-$			−1.92	
			$15\Gamma_8^-$			−1.88	
		155.21	$8\Gamma_7^-$			−1.68	
		155.35	$16\Gamma_8^-$			−1.61	
		155.46	$9\Gamma_7^-$			−1.55	
			$17\Gamma_8^-$			−1.53	
	155.51	155.51	$18\Gamma_8^-$		−1.26	−1.44	−1.47
		155.71	$19\Gamma_8^-$			−1.35	
$2p'$	194.08						
$3p'$	197.12						
$4p'$	198.20						

[a]Error is estimated to be ±0.006 meV for energies given to 3 decimal places and ±0.01 for those given to two decimal places.

[b]Calculated using Eq. (1).

[c]Calculated using the method of Ref. 6, namely, fixing the energy of line 7 to be −3.33 meV.

$2\Gamma_6^-$ and $6\Gamma_8^-$. Pajot *et al.*[6] associate line 6 with the $2\Gamma_6^-$ final state. The present transition energy for line 6, 153.29 meV, corresponds to a final-state energy of −3.62 meV (the method for obtaining energies of states from transition energies will be described below), which lies closer to that of the $6\Gamma_8^-$ state, namely, −3.63 meV, than it does to that of $2\Gamma_6^-$ state, namely, −3.70 meV. Taking into account also that the oscillator strength of the former state is greater than that of the latter state according to recent calculations[28,29] (although another recent calculation[30] indicates the opposite), the present data suggest line 6 should be associated with the 6 Γ_8^- final state, although this conclusion is not definite.

TABLE II. Ionization energies (in meV) of group III acceptors in silicon.

	B	Al	Ga	In
Ref. 54	45.71	70.18	74.05	156.90
Ref. 17	45.83	70.42	74.16	156.94
Ref. 5	44.39	69.03	72.73	155.58
Ref. 6	45.73	70.44	74.12	156.98
This work[a]	45.59	70.66	74.27	156.69

[a]The experimental transition energies used in this work are from Ref. 46 for Si(B) and from Ref. 5 for Si(Al) and Si(Ga).

The recent experimental[6] and theoretical[28–30] work concurs with the present identification of the lines labeled $6A$, 7, and 8 with transitions to final states $2\Gamma_7^-$, $7\Gamma_8^-$, and $3\Gamma_6^-$, respectively. The final states corresponding to the next four lines, of transition energies 154.21, 154.47, 154.72, and 154.94 meV, are not certain, but are tentatively assigned here to be $8\Gamma_8^-$, $4\Gamma_7^-$, $11\Gamma_8^-$, and $5\Gamma_7^-$, respectively. The identification of the second and fourth of these lines is established on the basis of oscillator strength as well as energy and must be regarded as being more certain than the identification of the first and third of these lines. In contrast, Pajot *et al.*[6] associate these four transitions with the states $9\Gamma_8^-$, $10\Gamma_8^-$, $13\Gamma_8^-$, and $6\Gamma_7^-$, respectively. The final line observed in the present experiments, having an energy of 155.51 meV, has a binding energy beyond those calculated by Buczko and Bassani;[29] Pajot *et al.*[6] identify this transition with the final state $18\Gamma_8^-$.

Three transitions of the $p_{1/2}$ series, namely, $2p'$, $3p'$, and $4p'$, can be seen in Fig. 1. Because of their interaction with the $p_{3/2}$ continuum, these transitions appear as broad and asymmetric features, and so they should be properly classified as Fano resonances,[4] but, of course, are distinct from those associated with the $p_{3/2}$ series. Comparing the present data with those of other group III acceptors, e.g., gallium[44] and boron[2] in silicon, it can be seen that the spectral line shapes of the $p_{1/2}$ transitions are less symmetric for the deeper acceptor.

In this investigation, 16 transitions of the $p_{3/2}$ series and 3 resonant transitions of the $p_{1/2}$ series have been observed (see Table I). The correlation between the observed transition energies and the calculated energies of the final states of the transitions is obtained in a manner similar to that given previously for Zn^- in germanium[45] and for boron in silicon.[46] If a plot is made of the theoretical energies calculated by Buczko and Bassani[29] for boron and aluminum in silicon against the present experimental transition energies of indium in silicon using only the well-resolved low-energy transitions having Γ_8^- final states, viz., lines 1, 2, 3, 5, and 7, very good linear fits with gradients close to unity result, as was the case for Zn^- in germanium.[43,45] Extrapolating these fits to zero theoretical energy gives the ionization energy ϵ_i. The values so obtained are listed in Table II. Also listed, for comparison, are the values of ϵ_i as obtained from other work using different methods. The result of the linear fit for the indium data gave the relation

$$\epsilon = -(166.61 \pm 0.55) + (1.0633 \pm 0.0037) h\nu, \qquad (1)$$

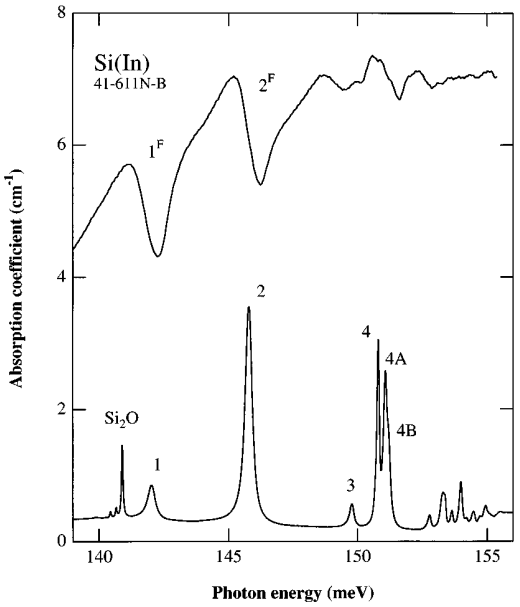

FIG. 3. The $p_{3/2}$ and Fano series of the spectrum of Fig. 1. The upper trace, showing the Fano resonances, has been shifted down in energy by the optical phonon energy, 64.35 meV, and the ordinate scaled up by a factor of 20.

where $h\nu$ and ϵ are the experimental transition energy and the theoretical energy of the corresponding final state, respectively, measured in meV. The values of the experimental energies of the final states given in the sixth column of Table I were determined using Eq. (1) and the observed transition energies.

It might be noted that the absorption spectrum of the $p_{3/2}$ series for a sample with a 50% greater indium concentration than that of the sample of Fig. 1 cut from the crucible-grown ingot (2789) shows two oxygen vibronic bands. One is at 149.50 meV (to the low-energy side of line 3), the so-called ''8μ'' band;[47] the other (on the low-energy side of line 1) is the strong ''9μ'' band.[47–49] Two other lines, both very weak, have been found in the $p_{3/2}$ spectrum: at 150.40 meV (to the low-energy side of line 4), and at 151.72 meV (to the high-energy side of line $4B$), and are here designated as X_1 and X_2, respectively. The genuineness of these weak features is confirmed by the fact that both split into two components under $\langle 100 \rangle$ compression, showing a behavior characteristic of electronic states. No transitions between states of the same parity have been observed in the absorption spectrum of group III acceptors in silicon before. Some of the even parity excited states of boron,[50] gallium,[50] and indium[17] in silicon have been determined from two-hole transitions in bound exciton photoluminescence spectra. The energy differences between the ground state and some even parity states, $2\Gamma_8^+$, $3\Gamma_8^+$, $4\Gamma_8^+$, and $5\Gamma_8^+$, have been given as 137.72 ± 0.5, 148.82 ± 0.3, 152.46 ± 0.3, and 154.35 ± 0.3 meV, respectively, for indium-doped silicon.[17] Comparing these values with the energies of X_1 and X_2, it is conjectured that these weak features relate to the transitions having final states $3\Gamma_8^+$ and $4\Gamma_8^+$, respectively, but this identification is not final.

Figure 3 presents the correlation between the $p_{3/2}$ series

TABLE III. Parameters for 1^F and 2^F of Si(In). Units are meV, except for q, which is dimensionless.

Feature	$h\nu_0$	$h\nu_0-\hbar\omega_{\rm opt}$	$h\nu^{\rm a}$	f	q	Γ
1^F	206.16±0.01	141.8±0.1	142.023±0.006	−0.2±0.1	−0.85±0.02	1.16±0.03
2^F	210.14±0.03	145.8±0.1	145.791±0.006	0.0±0.1	−0.86±0.04	1.11±0.06

[a]Experimental transition energy; see second column of Table I.

and the Fano series. The upper trace, showing the Fano resonances, has been shifted down by the zone-center optical phonon energy of 64.35 meV (Ref. 39) and scaled up in the ordinate by a factor of 20. The Fano resonance features 1^F and 2^F are well resolved and clearly related to lines 1 and 2 of the $p_{3/2}$ series. The Fano resonance associated with line 3 is complicated by a smaller resonance on its high-energy side, which may relate to X_1. It may be noted that the resonant strengths of 1^F and 2^F are very similar, even though the intensity of line 1 is much smaller than that of line 2; similarly, the intensities of lines 4 and $4A$ are much stronger than that of line 1 in the $p_{3/2}$ series, but the Fano resonances of lines 4 and $4A$ are very weak compared to 1^F. These observations confirm that the resonance strength does not follow the oscillator strength of the parent transition and suggest that the lower the energy of the excited state, i.e., the more localized the wave function, the stronger the Fano resonance. This is in keeping with the optical phonon involved being produced locally in an environment where there is no center of inversion, viz., the locale of the impurity, it being well known that optical phonons cannot be excited singly in a crystal with a center of inversion such as silicon. This is also the case regarding G^F and D^F in the spectra of Zn^- in germanium.[45] The ''straight line'' method developed previously,[35] viz., determining the resonance position by the intercept of the resonant feature and the straight line joining the maximum and minimum of the feature, has been employed to determine the parameters of the well-defined Fano resonances 1^F and 2^F. In determining $h\nu_{\rm max}$, $h\nu_{\rm min}$, and $h\nu_0$, and thus the values of q, Γ, and f, average values were taken from four spectra from four independent measurements of two samples with different indium concentrations. The results are given in Table III. The shapes of 1^F and 2^F are very similar and so are their respective Fano parameters q, Γ, and f. In contrast, the first two Fano transitions of Zn^- in germanium, G^F and D^F, have quite dissimilar parameters (see Table I of Ref. 35), even though the two bound hole transitions involved in the two materials correspond in that they are to the first two excited states, viz., $1\Gamma_8^-$ and $2\Gamma_8^-$. It might be pointed out that in the case of Zn^- in germanium the hole-phonon compound state interacts only with the $p_{3/2}$ continuum, while for indium in silicon, it interacts with the $p_{1/2}$ continuum as well.

An attempt was made to detect Fano resonances associated with the $p_{1/2}$ series, which are expected to occur at ~260 meV; no resonances were observed.

IV. EFFECT OF UNIAXIAL STRESS

Piezospectroscopic observations have been made with an applied force **F** along either a ⟨111⟩, ⟨110⟩, or ⟨100⟩ axis and the electric vector **E** of the radiation polarized either parallel ($\mathbf{E}_\parallel$) or perpendicular ($\mathbf{E}_\perp$) to **F**. In this section, the detailed stress behavior of transitions is given for lines $2p'$, $3p'$, and $4p'$ of the $p_{1/2}$ series, lines 1, 3, and 4 of the $p_{3/2}$ series, and the Fano resonances. The first quantitative measurements for the splitting of line $2p'$ of In under ⟨111⟩, ⟨110⟩, and ⟨100⟩ compression have been made, as well as the first quantitative observation of components 1.1, 1.2, 2.4 and of lines 3, 4, $4A$, and $4B$ under ⟨111⟩ and/or ⟨100⟩ compression. In determining the deformation potential constants, the elastic compliance coefficients given by Hall[51] have been used. The piezospectra for the transitions of line 5 and higher lines in the $p_{3/2}$ series have also been obtained, but these are composed of very many relatively weak features. The details of these will not be presented or discussed here.

A. Piezospectroscopy of the $p_{1/2}$ series

The stress behavior of the $p_{1/2}$ series is simpler than that of the $p_{3/2}$ series and so will be discussed first. Each line splits into two under the application of stress and yields the ground-state splitting directly. The order of the sublevels of the ground state is determined uniquely from the polarization features of the $p_{1/2}$ doublets.[7]

In Fig. 4 are shown the piezospectra of the $p_{1/2}$ series under ⟨111⟩, ⟨110⟩, and ⟨100⟩ compressive stresses of similar but slightly different magnitudes. The $p_{1/2}$ spectra for ⟨111⟩ and for ⟨110⟩ compression show clearly the effect of stress on the $2p'$, $3p'$, and $4p'$ lines. The sample used for ⟨100⟩ compression was less pure and gave a spectrum that showed only the $2p'$ transition clearly. For $\mathbf{F}\|\langle 111\rangle$, the high-energy components of the $2p'$, $3p'$, and $4p'$ lines appear for both polarizations, while the low-energy components are observed only for $\mathbf{E}_\perp$; the intensity of each low-energy component decreases with stress, indicating that the

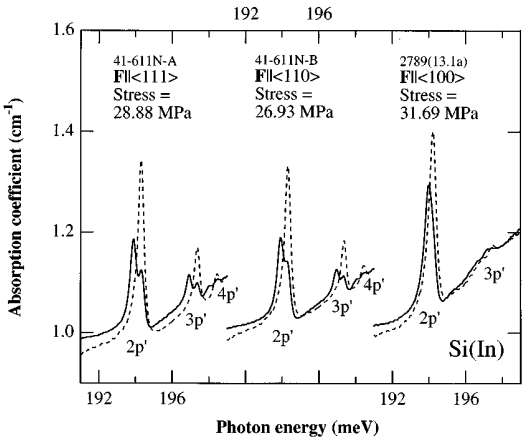

FIG. 4. Effect of ⟨111⟩, ⟨110⟩, and ⟨100⟩ compression on the lines $2p'$, $3p'$, and $4p'$.

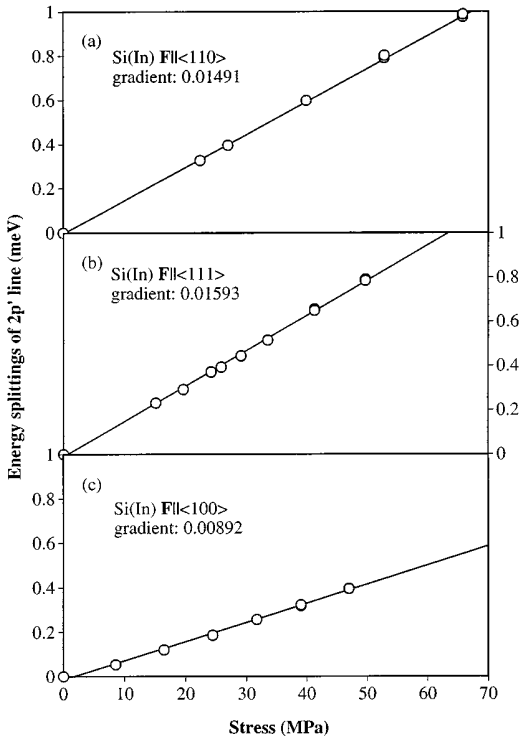

FIG. 5. Stress dependence of the splitting of the $2p'$ components for $\mathbf{F}\|\langle 111\rangle$, $\langle 110\rangle$, and $\langle 100\rangle$. The straight lines shown represent least-squares fits.

final states of these transitions are either a Γ_6 or a Γ_7 state. It can be seen from the observed polarization pattern that the order of the sublevels of the ground state is that shown in Fig. 1(a) of Ref. 34, viz., the energy of sublevel Γ_5 $(1\Gamma_8^+)$ + Γ_6 $(1\Gamma_8^+)$ $\equiv$ Γ_{5+6} $(1\Gamma_8^+)$ is greater than that of Γ_4 $(1\Gamma_8^+)$.

In Fig. 5, the ground-state splittings as obtained from the splittings of the $2p'$ line are presented as a function of stress for the three directions of applied force. The energy of the low-energy component for $\mathbf{E}_\perp$ under $\langle 100\rangle$ compression was determined by least-squares fitting a Lorentzian curve to the spectra and used, together with the value of the $\mathbf{E}_\parallel$ component, to evaluate the ground-state splitting for $\mathbf{F}\|\langle 100\rangle$; this process is reasonably direct since the energy of the $\mathbf{E}_\parallel$ component can be used to give that of the high-energy $\mathbf{E}_\perp$ component. The straight lines passing through the data points in Fig. 5 represent least-squares fits; these fits give the stress dependence of the energy splittings, Δ'_{111}, Δ'_{100}, and Δ'_{110}, as 0.01593 ± 0.00027, 0.00892 ± 0.00009, and 0.01491 ± 0.00010 meV/MPa, respectively. From these values the deformation potential constants for the ground state have been deduced to be $d_0 = -2.21\pm0.04$ eV and $b_0 = -0.46\pm0.03$ eV (see Table IV). The relation of the splittings of the same state under $\langle 111\rangle$, $\langle 100\rangle$, and $\langle 110\rangle$ compressions is[7]

$$\Delta_{110}=\tfrac{1}{2}(\Delta_{100}{}^2+3\Delta_{111}{}^2)^{1/2}. \qquad (2)$$

By using this relation with the data from the well-resolved ground-state splittings under $\langle 111\rangle$ and $\langle 110\rangle$ compressions, a value of $b_0 = -0.58\pm0.09$ eV is obtained, which may be compared with the above value of b_0 deduced directly from the splitting of the $2p'$ line under $\langle 100\rangle$ compression. Both values of b_0 are approximately half the magnitude of the value given by Chandrasekhar *et al.*,[7] which was determined indirectly under the assumption of ''stress isotropy'' for the ground-state splitting. The different gradients of the stress splittings of the $2p'$ components shown in Fig. 5 suggest that ''stress isotropy'' does not hold for indium in silicon.

TABLE IV. Comparison of deformation potential constants obtained by theory and experiments for Si(In). Units are eV.

	Si(III)	Si(In)	
	Theory[a]	Previous work[b]	This work
b_0	-1.39	-0.98 ± 0.03	-0.46 ± 0.03
			-0.58 ± 0.09 [c]
b_1	-0.03	~0	-0.70 ± 0.19 [c]
b_2	1.09	1.76 ± 0.10	1.09 ± 0.03
			1.18 ± 0.17 [c]
$\lvert b_3\rvert$	0		0.91 ± 0.10 [c]
d_0	-4.17	-2.68 ± 0.15	-2.21 ± 0.04
d_1	-1.84	-3.22 ± 0.25	-1.84 ± 0.11
d_2	2.04	3.54 ± 0.25	1.82 ± 0.03
d_3	-1.70		-1.53 ± 0.05

[a]Reference 19.
[b]Reference 7.
[c]Values derived using Eq. (2).

Under $\langle 110\rangle$ compression, a similar pattern for the $2p'$ and $3p'$ splittings to that obtained under $\langle 111\rangle$ compression was observed. The low-energy components of $2p'$ and $3p'$ for parallel polarization made their appearance only when stresses above 50 MPa were applied. Their intensities, however, were still very low. These components are expected to be observed since the selection rules permit all transitions for $\mathbf{F}\|\langle 110\rangle$.

B. Piezospectroscopy of the $p_{3/2}$ series and Fano resonances

1. Applied force along a $\langle 111\rangle$ axis

a. $p_{3/2}$ spectrum. The effect of uniaxial compressive stress for $\mathbf{F}\|\langle 111\rangle$ on some of the lines of the $p_{3/2}$ series is shown in Fig. 6 and the lower part of Fig. 7. The stress dependence of the resolved components of the transitions is given in Fig. 8. In this figure, the lines drawn through the data points are the results of least-squares fits. For line 1, four stress components, one for $\mathbf{E}_\parallel$ and three for $\mathbf{E}_\perp$, are observed. The analysis of these components confirms unambiguously the order of the energy sublevels, viz., the sublevels of the $1\Gamma_8^-$ excited state are in the same order as those of the $1\Gamma_8^+$ ground state, with the Γ_4 sublevels being lower in energy than the Γ_{5+6} sublevels. The order of the sublevels of the ground state is the same as that obtained from the polarization features of the $p_{1/2}$ lines. The component 1.1, of lowest energy, is not resolved at higher stresses because of its low intensity due to depopulation of the upper stress-induced ground state and also because of overlap with the oxygen lines. The intensity of component 1.3 is either zero or very weak for $\mathbf{E}_\parallel$; this implies that $u_1\approx1$.[34] The energy differences of the components 1.2 and 1.4, and of the components

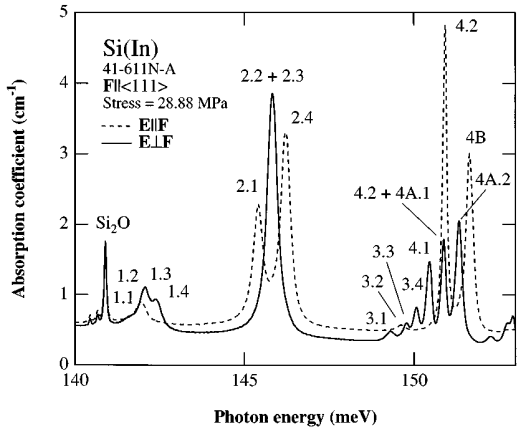

FIG. 6. The $p_{3/2}$ spectrum for $\mathbf{F}\|\langle 111\rangle$ and a stress of 28.88 MPa.

1.1 and 1.3, are essentially the same as those of the stress-induced components of $2p'$ and $3p'$, that is, the ground-state splitting. The separation of components 1.3 and 1.4 (or 1.1 and 1.2) gives the splitting of the $1\Gamma_8^-$ state. This splitting is used to obtain the deformation potential constant d_1. This value is given in Table IV and is believed to be more reliable than the previous result,[7] which is included in Table IV for comparison. The present result is identical to the theoretical value.[19]

Line 2 splits into two components for $\mathbf{E}_\parallel$ and three for $\mathbf{E}_\perp$, with the highest-energy component, 2.4, common to both polarizations (see Figs. 7 and 8). The stress behavior of this line has been studied comprehensively previously,[2,7] leaving no ambiguity in the stress-induced polarization pattern and in the ordering of the energy sublevels. The well-resolved data for components 2.1 and 2.4, and the values of the ground-state splitting obtained from the spacing of 2.1 and 2.3 and from the $2p'$ splitting, have been used to calculate the deformation potential constant d_2 of the $2\Gamma_8^-$ state. This value is given in Table IV along with the value obtained previously. The polarization pattern of line 3, which has not been analyzed before, is the same as that of line 1. It follows that the order of the sublevels of the $3\Gamma_8^-$ state is the same as that of the $1\Gamma_8^-$ state. The value of d_3 obtained is listed in Table IV. Since component 3.3 is not observed for $\mathbf{E}_\parallel$ it can be concluded that $u_3 \approx 1$, as was the case for u_1. The calculated[19] values of u_1 and u_3 are 1 and 0.97, respectively, in excellent agreement with the experiment.

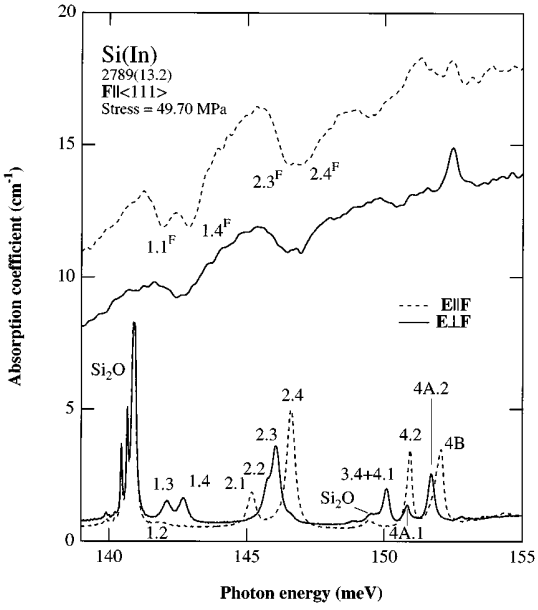

FIG. 7. The spectra of the $p_{3/2}$ and Fano series for $\mathbf{F}\|\langle 111\rangle$ and a stress of 49.70 MPa. The axis at the left applies to the $p_{3/2}$ series. The Fano spectra (upper two spectra) have been shifted down in energy by 64.35 meV and their ordinates scaled up by a factor of 20.

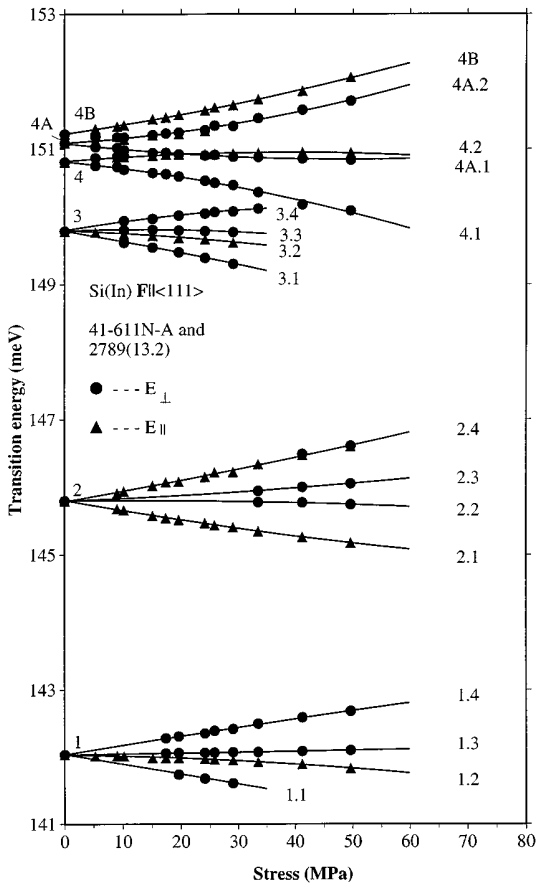

FIG. 8. Stress dependence of the components of the $p_{3/2}$ transitions for $\mathbf{F}\|\langle 111\rangle$. The lines shown represent least-squares fits.

The effect of stress further complicates the appearance of the closely spaced lines 4, $4A$, and $4B$. For $\mathbf{F}\|\langle 111\rangle$, four $\mathbf{E}_\perp$ and three $\mathbf{E}_\parallel$ components of this group were distinguished. Both line 4 and line $4A$ split into doublets with separations equal to the ground-state splitting. Only one $\mathbf{E}_\parallel$ component was seen for each of these lines. The energy of these components is the same as that of the respective high-energy $\mathbf{E}_\perp$ components. This is the typical polarization pattern of transitions from a Γ_8 ground state to a Γ_6 or Γ_7 excited state under a $\langle 111\rangle$ compression;[34] however, both a Γ_6 and a Γ_7 final state theoretically exhibit the same polarization pattern, which precludes unambiguously identifying

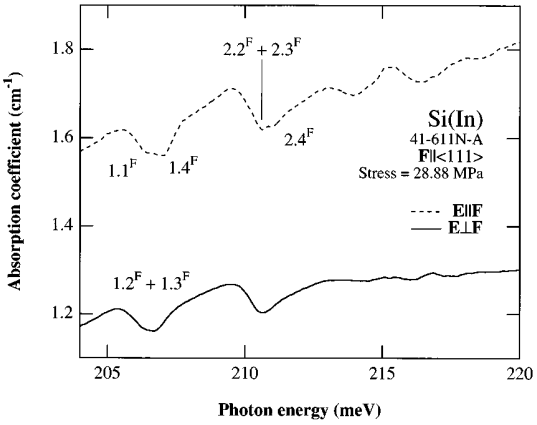

FIG. 9. The Fano spectrum for $\mathbf{F}\|\langle 111\rangle$ and a stress of 28.88 MPa.

the final states for these two lines from this observation. The intensities of components 4.1 and $4A.1$ decrease with stress as a consequence of the depopulation of the stress-induced upper sublevel of the ground state. The energies of the components of lines 4, $4A$, and $4B$ as a function of stress are shown in Fig. 7; data obtained from two samples are included.

b. Fano resonances. Figure 7 also presents the correlation between the $p_{3/2}$ series and the Fano series for $\mathbf{F}\|\langle 111\rangle$. The spectra of the Fano resonances have been shifted down in energy by the zone-center optical phonon energy, and the absorption coefficient has been scaled up by a factor of 20. Figure 9 shows the Fano resonances under $\langle 111\rangle$ compression with a stress of 28.88 MPa. Figure 7 was obtained from the less pure sample (ingot 2789), and shows an unidentified absorption peak at 216.81 meV. The splitting of the Γ_5 phonon for this direction and magnitude of compression is too small to be determined from the Fano components without very high-resolution measurements. At the maximum stress employed, viz., 49.7 MPa, the phonon splitting is $\sim$0.006 meV. Figure 10 combines the stress dependence of the energies of lines 1 and 2 of the $p_{3/2}$ series with that of lines 1^F and 2^F of the Fano series. For ease of comparison, the energies of the components of the Fano series have been shifted down by 64.35 meV. The fits to the data are shown as full lines for the $p_{3/2}$ components and as dashed lines for the Fano components. The energies of the minima were used to follow the stress dependence of the Fano resonances, a method validated earlier.[43,52] The two $\mathbf{E}_\parallel$ components of 1^F may be identified as 1.1^F and 1.4^F, since their stress dependencies are similar to those of components 1.1 and 1.4 of the $p_{3/2}$ series. The main uncertainty in these measurements arises from the overlapping of the closely spaced, broad resonance features. For $\mathbf{E}_\perp$, the Fano resonances of the stress components of line 1 are not well resolved. The width of the feature observed suggests that there are at least two Fano stress components involved. The observed components of 2^F are identified as $2.2^F + 2.3^F$ and 2.4^F, since they follow the stress behavior of the corresponding $p_{3/2}$ lines. In the $p_{3/2}$ series, the 1.1, 1.4, 2.2, and 2.3 components for $\mathbf{E}_\parallel$ are forbidden by symmetry. The presence of 1.1^F, 1.4^F, and $2.2^F + 2.3^F$ for $\mathbf{E}_\parallel$ is permitted by the

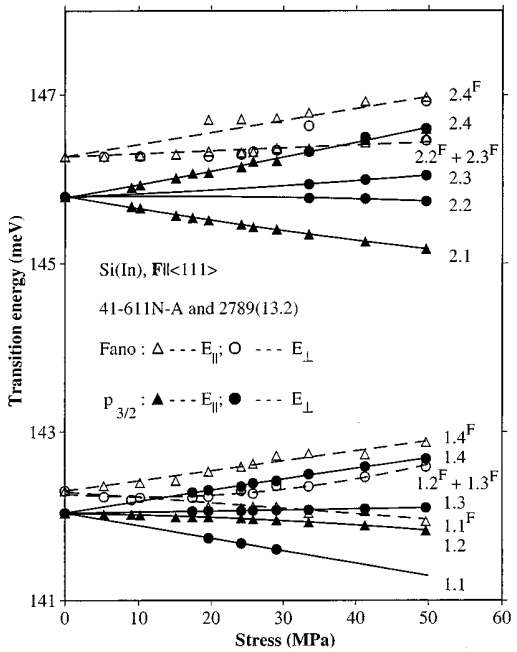

FIG. 10. Stress dependence of the components of the 1, 2, 1^F, and 2^F transitions for $\mathbf{F}\|\langle 111\rangle$. The Fano series has been shifted down in energy by 64.35 meV. The lines shown represent least-squares fits.

relaxation of the selection rules resulting from the involvement of the phonon.[52]

2. Applied force along a ⟨110⟩ axis

a. $p_{3/2}$ spectrum. In Fig. 11 and the lower part of Fig. 12 is presented the effect of a compressive force, parallel to the [110] axis, on part of the $p_{3/2}$ series. Here $\mathbf{q}\|[111]$, where $\mathbf{q}$ is the wave vector of the radiation. As for $\langle 111\rangle$ compression, only spectra for lines 1 to $4B$ of the $p_{3/2}$ series are shown. The stress dependence of the energies of the resolved components of these lines is given in Fig. 13.

All the transitions from the stress-induced ground-state sublevels to the excited-state sublevels are permitted by the

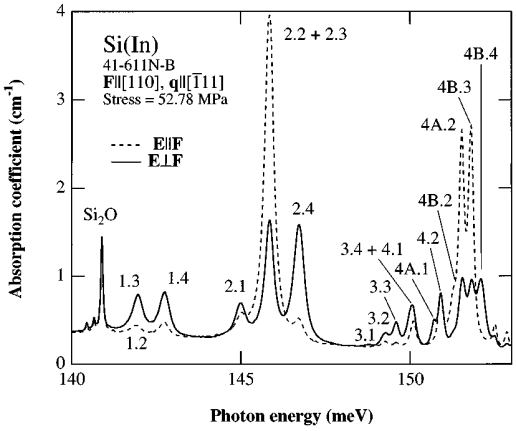

FIG. 11. The $p_{3/2}$ spectrum of Si(In) for $\mathbf{F}\|[110]$ and $\mathbf{q}\|[\bar{1}11]$ and a stress of 52.78 MPa.

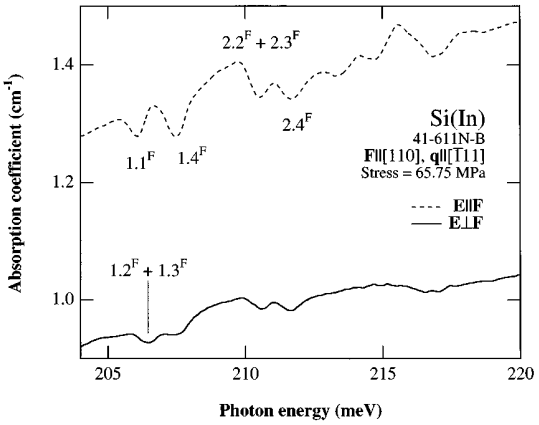

FIG. 12. The Fano spectrum for $\mathbf{F}\|[110]$ and $\mathbf{q}\|[\bar{1}11]$ and a stress of 65.75 MPa.

selection rules[34] for $\mathbf{F}\|\langle 110\rangle$. The relative intensities of the transitions depend on the direction of light propagation $\mathbf{q}$, since the crystal becomes orthorhombic under $\langle 110\rangle$ compression.[34,53] The number of stress components observed for lines 1, 2, and 3 is consistent with the fact that all these lines arise from transitions to Γ_8 final states. The energy spacings between components 1.2 and 1.4 and between components 1.1 and 1.3 are found to be the same and agree with the value of Δ'_{110}, the ground-state splitting, as determined from the stress splitting of the $2p'$ transition. The splitting of the $1\Gamma_8^-$ state then can be deduced from the separation of components 1.3 and 1.4 (or components 1.1 and 1.2). Three spectral lines were observed for line 2 for each polarization and for both polarizations the position of the strongest line, labeled 2.2+2.3, is almost unchanged with stress (see Figs. 11 and 12). This suggests that the stress components 2.2 and 2.3 are almost coincident in energy and that the splittings of the ground state and the $2\Gamma_8^-$ excited state are almost equal, which is confirmed by the fact that the energy spacings of components 2.4 and (2.2+2.3) and of components (2.2+2.3) and 2.1 are essentially the same as the ground-state splitting. For line 3, the separation of components 3.2 and 3.4 and of components 3.1 and 3.3 is that of the ground-state splitting. The splitting, $\Delta_{110}^{(3)}$, of the $3\Gamma_8^-$ state, the final state of line 3, has been obtained from the difference in energy of components 3.3 and 3.4. Using this and the result for $\Delta_{111}^{(3)}$ in Eq. (2) the magnitude of the deformation potential constant b_3 has been evaluated; this is found to be 0.91 ± 0.10 eV, a value significantly different from that calculated (see Table IV). The stress components of lines 4 and 4*A* are well defined and show behavior compatible with transitions from the ground state to final states, which are either Γ_6 or Γ_7.

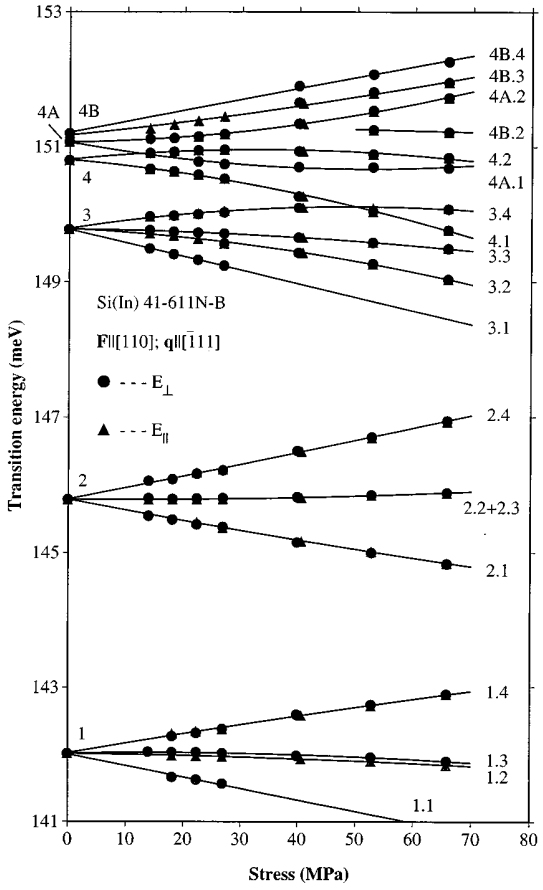

FIG. 13. Stress dependence of the components of the $p_{3/2}$ transitions for $\mathbf{F}\|[110]$ and $\mathbf{q}\|[\bar{1}11]$. The lines shown represent least-squares fits.

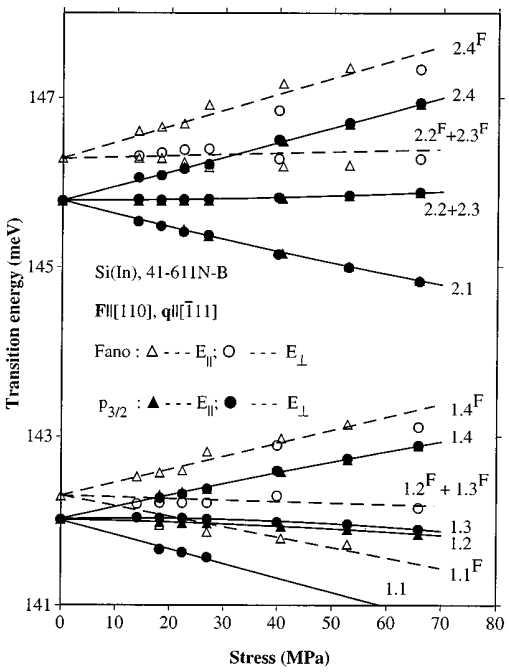

FIG. 14. Stress dependence of the components of the 1, 2, 1^F, and 2^F transitions for $\mathbf{F}\|[110]$ and $\mathbf{q}\|[\bar{1}11]$. The Fano series has been shifted down in energy by 64.35 meV. The lines shown represent least-squares fits.

b. Fano resonances. In Fig. 12 are presented the effects of $\mathbf{F}\|[110]$ and $\mathbf{q}\|[\bar{1}11]$ on the Fano resonances. For comparison, the stress dependence of the energies of lines 1 and 2 of the $p_{3/2}$ series and of the lines 1^F and 2^F of the Fano series are shown in Fig. 14. The energies of the components of the Fano series have been shifted down by 64.35 meV in

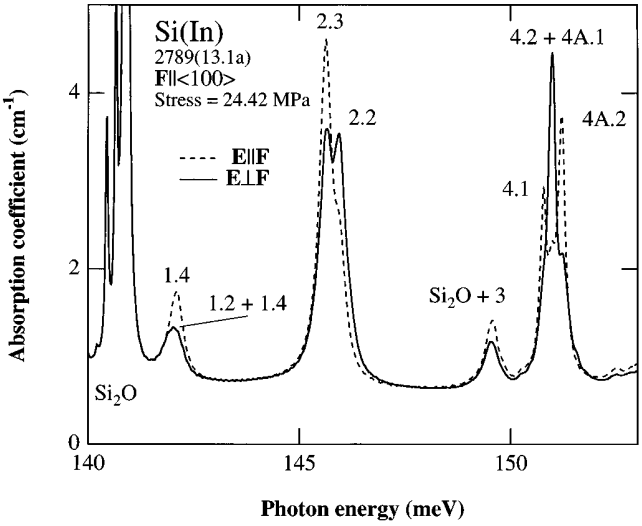

FIG. 15. The $p_{3/2}$ spectrum for $\mathbf{F}\|\langle 100\rangle$ and a stress of 24.42 MPa.

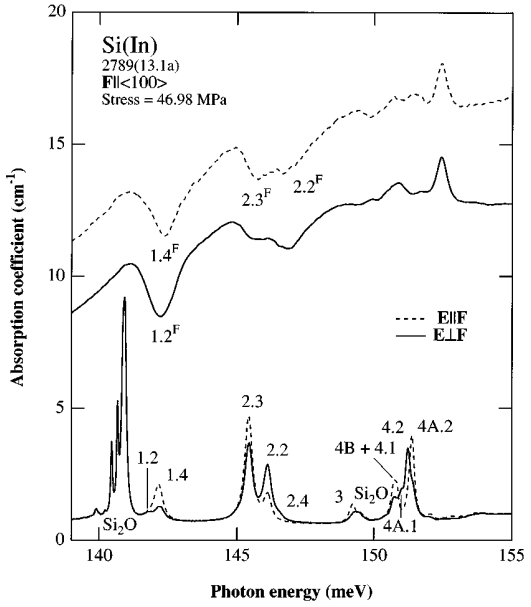

FIG. 16. The spectra of the $p_{3/2}$ and Fano series for $\mathbf{F}\|\langle 100\rangle$ and a stress of 46.98 MPa. The axis at the left applies to the $p_{3/2}$ series. The Fano spectra (upper two spectra) have been shifted down in energy by 64.35 meV and their ordinates scaled up by a factor of 20.

this figure. For 1^F, three stress components, 1.1^F, $(1.2^F+1.3^F)$, and 1.4^F can be clearly identified. Their stress dependence is similar to that of their $p_{3/2}$ counterparts. However, their relative strengths are different; the strongest $\mathbf{E}_\|$ component in the $p_{3/2}$ series, 1.2, does not appear in the Fano series at all. The 1^F components are comparable in intensity to the 2^F components, while in the $p_{3/2}$ series, the stress components of line 2 are much stronger than those of line 1. Due to their relatively close spacing, large width and low intensity, no quantitative analysis has been made of these stress-split Fano resonances.

3. Applied force along a ⟨100⟩ axis

a. $p_{3/2}$ spectrum. The effect of a $\langle 100\rangle$ compression on the $p_{3/2}$ spectrum is presented in Fig. 15 and the lower part of Fig. 16. The energies of the resolved stress-induced components of lines 1 to $4B$ are shown in Fig. 17 as a function of stress. The lines drawn through the data points are the results of least-squares fits.

For line 1, two components for $\mathbf{E}_\perp$ and one component for $\mathbf{E}_\|$ were observed (see Figs. 16 and 17), rather than the permitted four $\mathbf{E}_\perp$ components and two $\mathbf{E}_\|$ component,[34] leading to some uncertainty in labeling the observed components. The energies of the low-energy $\mathbf{E}_\perp$ components, 1.2, shown in Fig. 17 are those obtained by curve fitting the absorption lines and only for stresses greater than 30 MPa. Linear fitting to the data of 1.4 (both $\mathbf{E}_\perp$ and $\mathbf{E}_\|$) gives a gradient of 0.00276 ± 0.00028 meV/MPa and fitting the data to the low-energy component gives -0.00608 ± 0.00005 meV/MPa. The zero stress energy of line 1 is not included in these fits. The difference in gradient of these two fits, 0.00884 ± 0.00033 meV/MPa, gives the splitting of the two components, which is essentially the same as the stress dependence of the ground-state splitting as determined from the $2p'$ doublet, 0.00892 ± 0.00009 meV/MPa. The intensity of the low-energy $\mathbf{E}_\perp$ component decreases and that of the $\mathbf{E}_\|$ component increases with stress, a depopulation effect. It may be concluded that the low-energy $\mathbf{E}_\perp$ component is a transition from the upper sublevel and that the $\mathbf{E}_\|$ component is a transition from the lower sublevel of the ground state. The splitting of the $1\Gamma_8^-$ excited state has been estimated previously[7] as being very small. In the present work, the splittings of this state for $\mathbf{F}\|\langle 110\rangle$ and $\langle 111\rangle$ are found from the stress dependence of the energy difference between components 1.4 and 1.3 to be 0.01333 ± 0.00156 meV/MPa and 0.01322 ± 0.00079 meV/MPa, respectively, for these two orientations. These values permit an estimation of the splitting of the $1\Gamma_8^-$ state for $\mathbf{F}\|\langle 100\rangle$ using Eq. (2); this leads to a stress dependence of $\Delta_{100}^{(1)}$ of 0.01365 ± 0.00380 meV/MPa. The magnitude of the deformation potential constant, b_1, of the $1\Gamma_8^-$ state is then calculated to be 0.70 ± 0.19 eV, a value significantly larger than that predicted (see Table IV). It may be noted that $\Delta_{100}^{(1)}>\Delta'_{100}$. Taking into account the magnitude of the stress splittings and the depopulation effects it can be concluded that the sublevels of the $1\Gamma_8^-$ state and those of the ground state are in the same order. The labeling of the two components of line 1 as 1.2 and 1.4 is based on the above information and is different from that given previously,[2,7] where only one absorption line (currently labeled 1.4) was observed and identified as $1.3+1.4$, which led to $\Delta_{100}^{(1)}\approx 0$, a value close to that calculated.

The polarization pattern of line 2 is the same as that observed previously.[2,7] Two strong components for each polarization are seen. The appearance of the small shoulder labeled 2.4 in Fig. 16 supports the conclusions previously reached about the sublevels of the $2\Gamma_8^-$ state, i.e., the sublevels of this state are in the opposite order to those of the ground state, and the excited-state splitting is larger than the ground-state splitting. This is supported by the observation that the intensity of component 2.2 decreases relative to that

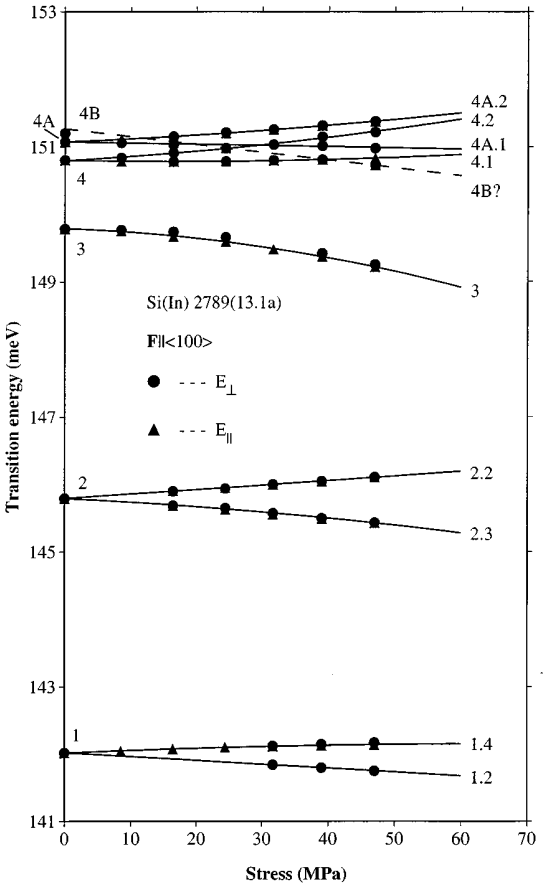

FIG. 17. Stress dependence of the components of the $p_{3/2}$ transitions for $\mathbf{F}\|\langle 100\rangle$. The lines shown represent least-squares fits.

of 2.3 with increasing stress (see Figs. 15 and 16). The labeling of the components of line 2 given by Onton, Fisher, and Ramdas[2] is adopted here. The deformation potential constant for the $2\Gamma_8^-$ state has been evaluated in two ways for comparison. One value was obtained directly from the data for $\langle 100\rangle$ compression, i.e., $\Delta_{100}^{(2)} = \text{``}2.2 - 2.3\text{''} + \Delta'_{100}$, the ground-state splitting, Δ'_{100}, being that deduced earlier from $2p'$. This yields $b_2 = 1.09 \pm 0.03$ eV. A second value was obtained from Eq. (2), giving a magnitude of $b_2 = 1.18 \pm 0.33$ eV. It can be seen that these two values agree. The ratios of b_2/b_0 from the two values of b_2 are -2.4 and -2.6, respectively, in good agreement with the estimation[2] that the $2\Gamma_8^-$ state splitting is about 2.5 times the ground-state splitting.

No detailed analysis could be made of the stress components of line 3 for $\mathbf{F}\|\langle 100\rangle$ due to the proximity of the weak oxygen line in the only sample available. The stress behavior of one component of line 3 is shown in Fig. 17. Since only one component is observed, it is not possible to determine either the magnitude or the sign of b_3, hence there is no comparison possible with the result deduced using $\Delta_{110}^{(3)}$ and $\Delta_{111}^{(3)}$.

It has been noted previously that compression along a $\langle 100\rangle$ axis reveals the most detail about the closely spaced C lines of Zn^- in germanium[43,52] and of gallium in germanium.[42] A similar situation may be expected for the complex 4, $4A$, and $4B$ of indium in silicon. In this investigation, however, the lines 4, $4A$, and $4B$ for $\mathbf{F}\|\langle 100\rangle$ were not as well resolved as those obtained under $\langle 111\rangle$ and $\langle 110\rangle$ compressions. Even so, sufficient information is available to determine which of the strong lines 4 and $4A$ is the transition to the $1\Gamma_6^-$ state and which is the transition to the $1\Gamma_7^-$ state. Given that the lower-energy sublevel of the ground state is Γ_7, the other being Γ_6, transitions to a final Γ_6 state will be characterized by two $\mathbf{E}_\perp$ components and one $\mathbf{E}_\|$ component, the $\mathbf{E}_\|$ component coinciding in energy with the higher-energy $\mathbf{E}_\perp$ component and having four times its intensity; the lower-energy $\mathbf{E}_\perp$ component has three times the intensity of the higher-energy one.[34] In contrast, transitions to a Γ_7 final state will have a common low-energy $\mathbf{E}_\|$ component and $\mathbf{E}_\perp$ component and an $\mathbf{E}_\perp$ component of higher energy, the respective intensities being in the ratios 4:1:3. The strong features observed in the line 4 complex under stress (see Figs. 15 and 16) are, in order of increasing energy, an $\mathbf{E}_\|$ component (4.1), an $\mathbf{E}_\perp$ component (4.2), and another $\mathbf{E}_\|$ component ($4A$.2). Both $\mathbf{E}_\|$ components coincide with weak $\mathbf{E}_\perp$ components. The strong central $\mathbf{E}_\perp$ component in this set is interpreted to be the superposition of the two stronger components of this polarization, which arise from the adjacent Γ_7 and Γ_6 states ($4A.1 + 4.2$). Taking thermal depopulation effects into account, the polarization features thus establish that line 4 arises from a transition to a Γ_7 state and line $4A$ arises from a transition to a Γ_6 state. This identification of line 4 with the $1\Gamma_7^-$ state and line $4A$ with the $1\Gamma_6^-$ state is used in Table I. Line $4B$ ($4\Gamma_8^-$) has a relatively low intensity at low stress, which ensures that it does not confuse the above analysis. The ground-state splitting can be deduced from the stress dependence of line 4 or $4A$. Only the energy difference of the stress components $4.2(\mathbf{E}_\perp)$ and $4.1(\mathbf{E}_\|)$ is used to evaluate Δ'_{100}. (Most values of the energies for the low-energy component of $4A$, i.e., $4A.1$, could only be obtained by curve fitting, which is thought to be less reliable.) If a linear fit is made to this energy difference, Δ'_{100}, as a function of stress, the result is 0.00894 ± 0.00034 meV/MPa, which is in excellent agreement with the value of 0.00892 ± 0.00009 meV/MPa obtained from the $2p'$ stress splitting. Only one stress-induced component of line $4B$ was observed. The unperturbed energy of line $4B$ shown in Fig. 17 was obtained from a purer sample (see Fig. 2) and is not included for the fit shown (dashed line). No detailed analysis can be made of this transition.

b. Fano resonances. Figure 16 shows the spectrum of the Fano resonances under $\langle 100\rangle$ compression and its correlation with the $p_{3/2}$ series. The stress dependence of the energies of the minima of the components of 1^F and 2^F is shown in Fig. 18, with the stress dependence of the components of lines 1 and 2 of the $p_{3/2}$ series included for comparison. As in the unperturbed spectrum, the Fano components associated with lines 1 and 2 of the $p_{3/2}$ series are the strongest; the weaker features identified as Fano resonances associated with lines 3 and 4, and an unidentified feature at higher energy, have not been analyzed. For line 1, for each polarization, only one Fano stress component was observed. These are labeled 1.2^F for $\mathbf{E}_\perp$ and 1.4^F for $\mathbf{E}_\|$. As can be seen in Fig. 18, the correlation with the $p_{3/2}$ components 1.2 and 1.4 is only fair.

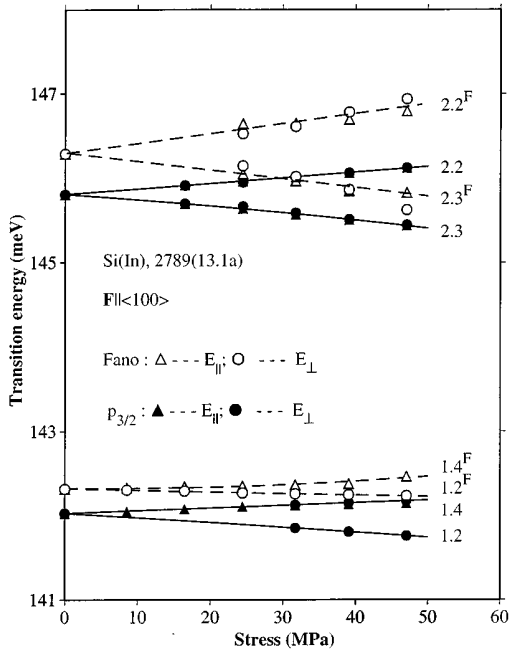

FIG. 18. Stress dependence of the components of the 1, 2, 1^F, and 2^F transitions for $\mathbf{F}\|\langle 100\rangle$. The Fano series has been shifted down in energy by 64.35 meV. The lines shown represent least-squares fits.

The energy separation between these two Fano resonances increases with stress but differs from that between the 1.2 and 1.4 components of the $p_{3/2}$ series. There are two stress components of 2^F for each polarization with a separation, however, larger than that of the $p_{3/2}$ counterparts with which they have been correlated. The deviation between these two associated series, Fano and $p_{3/2}$, for lines 1 and 2, is believed to be due to the uncertainty in analyzing the overlapped asymmetric Fano features. It may be noted that the parameter f, which is the measure of the strength of the coupling and represents a shift of the resonance position with respect to the energy of the compound state, is, in principle, energy dependent, as is the parameter q.[8] Variations in these parameters with stress may alter the energy of the observed resonances.

V. CONCLUSION

A detailed study has been made of the $p_{3/2}$ and $p_{1/2}$ Lyman series and the Fano resonances of indium in silicon. The experimental transition energies obtained here are in excellent agreement with previous measurements and the most recent calculations.

More detailed piezospectra have been obtained than in previous studies. This has allowed a reevaluation of the energy-level scheme and the stress behavior of various lines of the $p_{3/2}$ series. The results for line 2 are similar to those given in earlier work.[2,7] For line 1 under $\langle 100\rangle$ compression, the present analysis leads to the conclusion that the energy splitting of the final state is larger than that of the ground state, rather than about zero as estimated previously.[7] For $\mathbf{F}\|\langle 111\rangle$, the ordering of the stress-induced sublevels of the final states of lines 1 and 3 is the same as the ordering of those of the ground state and opposite to those of line 2. The analysis of the polarization pattern and stress behavior implies that for $\mathbf{F}\|\langle 100\rangle$ the sublevels of the final state of line 1 have similar order to the ground-state sublevels but opposite to those of line 2. The splitting of the final state of line 2 is about 2.5 times that of the ground state, as suggested previously.[2] More accurate values of the deformation potential constants, b and d, for the $1\Gamma_8^-$ and $2\Gamma_8^-$ states than previously and their first determination for the $3\Gamma_8^-$ state have been given. The stress behavior of lines 4 and $4A$ is clearly observed under both $\langle 111\rangle$ and $\langle 110\rangle$ compressions, while that for $\mathbf{F}\|\langle 100\rangle$ permits the final states of lines 4 and $4A$ to be unambiguously determined to be Γ_7^- and Γ_6^-, respectively. Although not discussed in the text, the stress behavior of line 5 for $\mathbf{F}\|\langle 111\rangle$ indicates that this is identical to that of lines 1 and 3; in particular, experimentally, it is deduced that these transitions all have a value of ~ 1 for the intensity parameter, u, in good agreement with the calculated values of 1, 0.97, and 0.97, respectively.[19]

The $p_{1/2}$ transitions, $2p'$, $3p'$, and $4p'$, appear as slightly asymmetric peaks. Their stress splittings directly give the ground-state splitting for the different orientations of $\mathbf{F}$ and can be used to aid in the interpretation of the behavior of the $p_{3/2}$ lines under stress. The ground-state splittings measured for $\mathbf{F}\|\langle 111\rangle$, $\langle 110\rangle$, and $\langle 100\rangle$ indicate that ''stress isotropy''[7] does not hold for indium in silicon.

The Fano resonances, arising from the interference between continuum states and those compounded from bound hole transitions and localized zone-center optical phonon states, show various typical line shapes. The energies at which the 1^F and 2^F resonances occur in the unperturbed absorption spectrum are deduced by a simple and accurate method,[35] which requires no detailed knowledge of the absorption background on which the resonances are superimposed. The other parameters characteristic of the Fano features, q, Γ, and f, are obtained. It is found that these are almost identical for the resonances 1^F and 2^F.

Piezospectroscopic observations of Fano resonances of indium, in silicon have been made. The Fano resonances experience splittings under stress similar to most of those of their counterparts in the $p_{3/2}$ series; there are some deviations from this pattern that are not understood. The phonon splittings due to stress are too small to be determined from the behavior of the Fano stress components in the experiments reported here. As expected, the intensity of the Fano series increases with sample concentration, while the relative intensities do not strictly follow those of the $p_{3/2}$ series, as is evidenced by the relative strengths of 1^F and 2^F compared to their $p_{3/2}$ counterparts. It is interesting to note that the intensities of the lower-energy Fano resonances are stronger relative to the other members of the series than are their $p_{3/2}$ counterparts. Fano resonances in impurity-doped silicon, generally speaking, provide additional information about some weak and/or even transition-forbidden excitations in the $p_{3/2}$ absorption spectra, leading to a fuller understanding of the optical processes involved.

ACKNOWLEDGMENTS

The authors are indebted to Professor A. K. Ramdas and Professor B. Pajot for provision of the indium-doped silicon

used in this work. The ingot labeled 2789 was obtained from Professor Ramdas and was purchased from Texas Instruments[2,7] while that labeled 41-611N was obtained from Professor Pajot.[6] This work was supported in part by the Australian Research Council and the University of Wollongong.

[1] H. J. Hrostowski and R. H. Kaiser, J. Phys. Chem. Solids **4**, 148 (1958).
[2] A. Onton, P. Fisher, and A. K. Ramdas, Phys. Rev. **163**, 686 (1967).
[3] S. Zwerdling, K. J. Button, B. Lax, and L. M. Roth, Phys. Rev. Lett. **4**, 173 (1960).
[4] A. Tardella and B. Pajot, J. Phys. (Paris) **43**, 1789 (1982).
[5] D. W. Fischer and J. J. Rome, Phys. Rev. B **27**, 4826 (1983).
[6] B. Pajot, I. L. Beinikhes, Sh. M. Kogan, M. G. Novak, A. F. Polupanov, and C. Song, Semicond. Sci. Technol. **7**, 1162 (1992).
[7] H. R. Chandrasekhar, P. Fisher, A. K. Ramdas, and S. Rodriguez, Phys. Rev. B **8**, 3836 (1973).
[8] U. Fano, Phys. Rev. **124**, 1866 (1961).
[9] K. L. Bhatia, Can. J. Phys. **49**, 374 (1971).
[10] T. C. Chandler, R. J. Spry, G. J. Brown, J. J. Rome, and R. J. Harris, Phys. Rev. B **26**, 6588 (1982).
[11] R. Baron, M. H. Young, and T. C. McGill, Solid State Commun. **47**, 167 (1983).
[12] Y.-C. Chang and T. C. McGill, Solid State Commun. **47**, 171 (1983).
[13] A. Baldereschi and N. O. Lipari, Phys. Rev. B **8**, 2697 (1973).
[14] A. Baldereschi and N. O. Lipari, Phys. Rev. B **9**, 1525 (1974).
[15] A. Baldereschi and N. O. Lipari, in *Proceedings of the 13th International Conference on the Physics of Semiconductors*, edited by F. G. Fumi (Tipografia Marves, Rome, 1976), p. 595.
[16] N. O. Lipari and A. Baldereschi, Solid State Commun. **25**, 665 (1978).
[17] N. O. Lipari, A. Baldereschi, and M. L. W. Thewalt, Solid State Commun. **33**, 277 (1980).
[18] N. Binggeli, A. Baldereschi, and A. Quattropani, in *Shallow Impurities in Semiconductors 1988*, edited by B. Monemar, IOP Conf. Proc. No. 95 (Institute of Physics and Physical Society, London, 1989), p. 521.
[19] R. Buczko, Nuovo Cimento **9D**, 669 (1987).
[20] R. Buczko and F. Bassani, in *Shallow Impurities in Semiconductors 1988* (Ref. 18), p. 107.
[21] Sh. M. Kogan and A. F. Polupanov, Solid State Commun. **27**, 1281 (1978).
[22] A. F. Polupanov and Sh. M. Kogan, Fiz. Tekh. Poluprovodn. **13**, 2338 (1979) [Sov. Phys. Semicond. **13**, 1368 (1979)].
[23] Sh. M. Kogan and A. F. Polupanov, Zh. Eksp. Teor. Fiz. **80**, 394 (1981) [Sov. Phys. JETP **53**, 201 (1981)].
[24] A. F. Polupanov and R. Taskinboev, Fiz. Tekh. Poluprovodn. **18**, 279 (1984) [Sov. Phys. Semicond. **18**, 173 (1984)].
[25] I. L. Beinikhes, Sh. M. Kogan, A. F. Polupanov, and R. Taskinboev, Solid State Commun. **53**, 1083 (1985).
[26] A. F. Polupanov and R. Taskinboev, Fiz. Tekh. Poluprovodn. **22**, 112 (1988) [Sov. Phys. Semicond. **22**, 68 (1988)].
[27] I. L. Beinikhes and Sh. M. Kogan, in *Shallow Impurities in Semiconductors 1988* (Ref. 18), p. 161.
[28] N. Binggeli and A. Baldereschi, Solid State Commun. **66**, 323 (1988).
[29] R. Buczko and F. Bassani, Phys. Rev. B **45**, 5838 (1992).
[30] I. L. Beinikhes, Sh. M. Kogan, M. G. Novak, and A. F. Polupanov, Mater. Sci. Forum **65-66**, 259 (1990).
[31] A. A. Kaplyanskii, Opt. Spect. (USSR) **16**, 557 (1964).
[32] G. E. Pikus and G. L. Bir, Fiz. Tverd. Tela **1**, 1642 (1959).
[33] G. L. Bir, E. I. Butikov, and G. E. Pikus, J. Phys. Chem. Solids **24**, 1467 (1963).
[34] S. Rodriguez, P. Fisher, and F. Barra, Phys. Rev. B **5**, 2219 (1972); **7**, 2889 (1973).
[35] G. Piao, R. A. Lewis, and P. Fisher, Solid State Commun. **75**, 835 (1990).
[36] V. J. Tekippe, H. R. Chandrasekhar, P. Fisher, and A. K. Ramdas, Phys. Rev. B **6**, 2348 (1972).
[37] N. R. Butler, Ph.D. thesis, Purdue University, 1974.
[38] E. H. Salib, Ph.D. thesis, University of Wollongong, 1982.
[39] P. A. Temple and C. E. Hathaway, Phys. Rev. B **7**, 3685 (1973).
[40] The symmetry labels are those in common usage and are defined in G. F. Koster, J. O. Dimmock, R. G. Wheeler, and H. Satz, *Properties of the Thirty-Two Point Groups* (MIT Press, Cambridge, MA, 1963). In the theoretical development of Lipari and Baldereschi the states are designated as belonging to $\underline{O}_h$ to retain the parity label, whereas in fact they belong to T_d.
[41] B. C. Covington, R. J. Harris, and R. J. Spry, Phys. Rev. B **22**, 778 (1980).
[42] R. E. M. Vickers, P. Fisher, and C. A. Freeth, Solid State Commun. **65**, 271 (1988).
[43] G. Piao, Ph.D. thesis, University of Wollongong, 1992.
[44] J. J. Rome, R. J. Spry, T. C. Chandler, G. L. Brown, B. C. Covington, and R. J. Harris, Phys. Rev. B **25**, 3615 (1982).
[45] G. Piao, R. A. Lewis, and P. Fisher, Mater. Sci. Forum **65-66**, 313 (1990).
[46] R. A. Lewis, P. Fisher, and N. A. McLean, in *Shallow Impurities in Semiconductors 1988* (Ref. 18), p. 95; Aust. J. Phys. **47**, 329 (1994).
[47] H. J. Hrostowski and R. H. Kaiser, Phys. Rev. **107**, 966 (1957).
[48] B. Pajot and J. P. Deltour, Infrared Physics **7**, 195 (1967).
[49] B. Pajot, J. Phys. Chem. Solids **28**, 73 (1967).
[50] M. L. W. Thewalt, Solid State Commun. **23**, 733 (1977).
[51] J. J. Hall, Phys. Rev. **161**, 756 (1967).
[52] G. Piao, R. A. Lewis, and P. Fisher, in *Proceedings of the 21st International Conference on the Physics of Semiconductors*, edited by Ping Jiang and Hou-Zhi Zeng (World Scientific, Singapore, 1992), p. 1609.
[53] R. L. Aggarwal and A. K. Ramdas, Phys. Rev. **137**, A602 (1965).
[54] A. K. Ramdas and S. Rodriguez, Rep. Prog. Phys. **44**, 1297 (1981).